AIAA JOURNAL
Vol. 46, No. 6, June 2008

Flow Reattachment and Vortex Re-formation on Oscillating Low-Aspect-Ratio Wings

E. Vardaki,* Z. Wang,† and I. Gursul‡
University of Bath, Bath,
England BA2 7AY, United Kingdom

DOI: 10.2514/1.32233

Effects of small-amplitude wing oscillations on flow reattachment and vortex re-formation in the poststall region were studied experimentally. Low-aspect-ratio delta and cropped delta wings with sweep angles in the range of $\Lambda = 20$–50 deg were tested. Effects of forcing frequency, amplitude, wing sweep angle, and mode of the wing oscillations were investigated. It was shown that wing oscillations at an appropriate frequency promotes the reattachment of the otherwise separated flow at poststall incidences. Moreover, with increasing frequency, leading-edge vortices develop with axial flow in the cores, followed by their breakdown. For an optimum range of Strouhal numbers, $Sr = 1$–2, vortex breakdown is delayed to a maximum distance from the apex. This range of Strouhal numbers compares well with the dominant frequencies of the shear layer instabilities. For sweep angles larger than 20 deg, the reattachment process is generic for all nonslender wings and there is an optimum range of Strouhal numbers.

Nomenclature

b	=	span
c	=	chord length
f	=	frequency
fc/U_∞	=	dimensionless frequency
Re	=	Reynolds number based on the chord length
Sr	=	Strouhal number, fc/U_∞
s	=	semispan
t	=	wing thickness
U_∞	=	freestream velocity
u	=	streamwise or chordwise velocity
v	=	spanwise component of velocity
x	=	chordwise distance
x_{bd}	=	chordwise location of vortex breakdown
y	=	spanwise distance
z	=	normal (to the wing surface) distance
α	=	angle of attack
Γ	=	circulation
$\Delta\alpha$	=	amplitude of pitch oscillations
$\Delta\phi$	=	amplitude of roll oscillations
Δy_w	=	distance between breakdown wakes at midchord
Λ	=	leading-edge sweep angle
ϕ	=	roll angle

I. Introduction

LOW-aspect-ratio wings are commonly used in many applications. Unmanned air vehicles and micro air vehicles often use low-sweep wings with sweep angles in the range of 35–55 deg. Better understanding of flow physics is needed for the development of flow control strategies for these wings. Although the flow topology over more slender wings, typically $\Lambda \geq 65$ deg, has been extensively studied [1–4], the flow over low-aspect-ratio wings has only recently attracted more attention [5–7].

A. Vortical Flows over Nonslender Wings

Leading-edge vortices develop close to the wing surface for nonslender delta wings. This results in strong viscous interactions with the boundary layer and a pronounced dependence of the flow structure on Reynolds number, in particular, at low angles of attack. For example, the time-averaged vortical flow exhibits an elongated form without complete roll up into a concentrated vortex at a low Reynolds number [5], however, vortices with large-scale concentration of vorticity develop with increasing Reynolds number [6,7]. The secondary vortex (of opposite sign) effectively splits the primary vortex into two separate concentrations of vorticity, resulting in a dual vortex structure at small angles of attack. As the angle of attack is increased, the primary vortex moves away from the surface; the structure then resembles more that of slender wings.

One of the distinct features of nonslender wings is that the primary attachment line occurs on the surface outboard of the symmetry plane, even when vortex breakdown is near the apex. In contrast, for highly swept wings, reattachment on the wing surface does not occur beyond very small angles of attack and therefore is difficult to manipulate [8]. For nonslender wings, reattachment of the flow on the wing surface can be manipulated. With increasing angle of attack, the reattachment line moves inboard toward the wing centerline. With further increase of angle of attack, reattachment is no longer observed, corresponding to the stall of the wing. Active and passive control of reattachment becomes possible in the poststall region, which is the main focus of this paper.

B. Flow Control in the Poststall Regime

The motivation of this work originated from recent studies [5,9–12], which reported great potential in controlling reattachment and increasing lift force for nonslender wings in the *poststall* region. The effect of perturbations on the aerodynamic forces in the *prestall* region seems very small [9,12], even though the manipulation of the separated shear layer is still possible [13]. It was shown by Yavuz et al. [13] that small-amplitude pitching oscillations of a nonslender wing ($\Lambda = 38.7$ deg) in the prestall regime ($\alpha = 10$ deg) cause changes in the near-surface flow structure, and the reattachment line moves outboard (closer to the leading edge), indicating earlier reattachment of the shear layer. However, for this prestall angle of attack, it appears that periodic pitching perturbations actually cause vortex breakdown to move upstream (Fig. 5 in [13]). As the effects of

Received 22 May 2007; revision received 30 January 2008; accepted for publication 7 February 2008.

*Research Officer, Department of Mechanical Engineering.
†Research Councils United Kingdom Academic Fellow, Department of Mechanical Engineering.
‡Professor, Department of Mechanical Engineering. Associate Fellow AIAA.

flow control appear to be small for prestall incidences [9,12], at least for the lift force, the main focus of this study is on the poststall regime.

C. Reattachment and Vortex Re-formation

For a wing with $\Lambda = 38.7$ deg in the poststall regime ($\alpha = 17$ deg), Yaniktepe and Rockwell [5] showed with dye visualization that the totally separated shear layer for the stationary wing becomes reattached near the wing symmetry plane for the oscillating wing. For the excited flow, dye flow visualization also indicates that vortex breakdown is at the apex of the wing; hence, there is not much axial flow within the reattachment region. Time-averaged streamlines suggest a recovery of the topological features of a leading-edge vortex in the crossflow plane, relative to those on the stationary wing. It is not clear whether vortex breakdown could be delayed and whether the re-formation of the vortex with axial flow is possible for this sweep angle.

Margalit et al. [9] showed that oscillatory blowing at the leading edge can enhance the lift in the poststall region of a delta wing with $\Lambda = 60$ deg, which is a transitional case between the slender and nonslender wings. Velocity measurements in a crossflow plane suggest the reattachment of the flow, but whether there is also axial flow or not is not known. Recent studies of flexible nonslender wings ($\Lambda = 40$–55 deg) reported lift enhancement in the poststall region [10–12]. This lift enhancement was associated with self-excited wing vibrations in the poststall region. These vibrations took place in an antisymmetric structural mode, and promoted reattachment of the separated shear layer to the wing surface. The structure of the reattached flow was found to be similar to a three-dimensional conical separation bubble in the time-averaged sense. An interesting observation was that, with increasing flexibility, a leading-edge vortex with axial flow develops within the reattachment region. Vortex breakdown is observed at a location downstream of the apex. This is called vortex re-formation in this study. It is not clear under which conditions vortex re-formation is possible.

D. Excitation Frequency

Although there are various sources of unsteadiness, such as shear layer instability (Kelvin–Helmholtz instability), vortex wandering, helical mode instability of vortex breakdown, oscillations of breakdown, vortex interactions, and vortex shedding, the only relevant one for flow control in the poststall regime is the shear layer instability [8]. Yaniktepe and Rockwell [5] suggested that the most effective frequency of excitation corresponded to the subharmonic of the dominant frequency in the region of the shear layer closest to the leading edge at $x/c = 0.8$. This frequency corresponds to $fc/U_\infty = 2.06$ and was the highest frequency tested in their experiments. However, this explanation is complicated by the fact that the frequency of the shear layer instabilities decreases with streamwise distance as the shear layer vortices shed conically [12]. Measurements indicate dominant frequencies in the range of $fc/U_\infty = 1$–5 for a rigid stalled wing with $\Lambda = 50$ deg. The Strouhal number of the dominant frequency of the structural vibrations was near unity for all nonslender wings.

In the experiments of Margalit et al. [9], the most effective frequency was found in the range of $fc/U_\infty = 1$–2 for $\Lambda = 60$ deg. At high frequencies, the performance was degraded, suggesting that an optimum range exists. It is not known whether there is an optimum range of excitation frequency for nonslender wings.

E. Objectives

The main objectives of this study are to investigate the two most important aspects (reattachment and vortex re-formation) and the effect of excitation frequency. The other aspects covered include the effect of wing sweep angle, wing planform shape, and spatial mode of excitation (symmetric vs antisymmetric wing oscillations). Initially, motivated by the antisymmetric vibration of the flexible wings that provide lift enhancement [10–12], experiments with a rigid delta wing undergoing small-amplitude of rolling motion were conducted in a water tunnel [14]. This approach has the advantage of independent control of the frequency parameter, which cannot be varied for a flexible wing without affecting the amplitude of vibrations. It was found that rigid delta wings undergoing small-amplitude oscillations in the poststall region exhibit many similarities to flexible wings, including the reattachment of the otherwise separated flow. A more interesting observation is the re-formation of the leading-edge vortices with axial flow and their consequent breakdown. These experiments with rigid oscillating wings were extended to various low-sweep wings in a subsequent conference paper [15]. Most recently, we have conducted further experiments. The purpose of this paper is to summarize our findings on the reattachment and vortex re-formation on oscillating low-aspect-ratio wings with sweep angles in the range of 20–50 deg. Flow visualization, particle image velocimetry (PIV), and laser Doppler velocimetry (LDV) measurements were used to study the unsteady aerodynamics of oscillating wings. Effects of forcing frequency, amplitude, wing sweep angle, and mode of the wing oscillations were investigated.

II. Experimental Methods

A. Facilities and Models

Experiments were conducted in a water-tunnel facility located at the University of Bath. The tunnel is an Eidetics Model 1520 free surface water tunnel, which has a $0.381 \times 0.508 \times 1.524$ m test section and can achieve speeds up to 0.45 m/s through a closed circuit continuous flow system. The tunnel has four viewing windows, three surrounding the working section and one downstream allowing axial viewing (see Fig. 1). The height of the test section above the floor allows flow visualization from below as well as from the sides. The tunnel also incorporates a dye system with six available dye tubes to enable flow visualization with different colors.

Experiments were conducted with low-aspect-ratio wings with various sweep angles and planform shapes as shown in Fig. 2. Simple delta wings have sweep angles $\Lambda = 50, 40, 30$ deg, whereas cropped delta wings have sweep angles $\Lambda = 50, 40, 30, 20$ deg. The span of the delta wings is the same ($b = 150$ mm) and the chord lengths are $c = 89, 63$, and 43 mm for $\Lambda = 50, 40, 30$ deg, respectively. For the cropped delta wings, the chord lengths are the same ($c = 100$ mm) and also the spans are the same ($b = 100$ mm). All wings are made of aluminum, have a thickness of $t = 2$ mm and bevel angles of 45 deg. An additional wing (simple delta, with $\Lambda = 50$ deg) with a larger thickness ($t = 4$ mm) was used in flow visualization experiments where the fluorescent dye was released from the slots at the leading edges. Flow visualization was performed for all wings, but detailed velocity measurements were conducted only for the simple delta wing with $\Lambda = 50$ deg. The models were mounted upsidedown in the tunnel using a sting projecting from the rear of the model, as shown in Fig. 1. A rolling mechanism was mounted with screws to the top of the mounting plate to produce the dynamic rolling motion of the delta

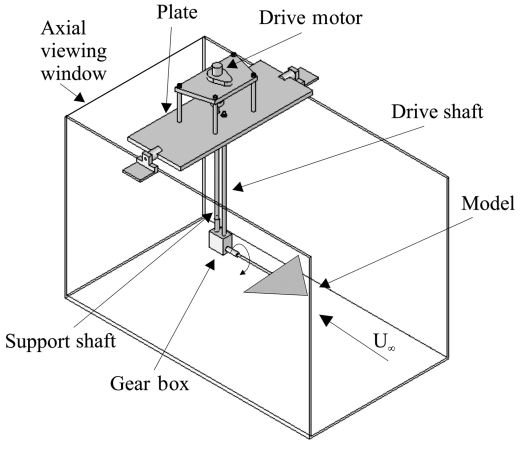

Fig. 1 Overview of experimental setup.

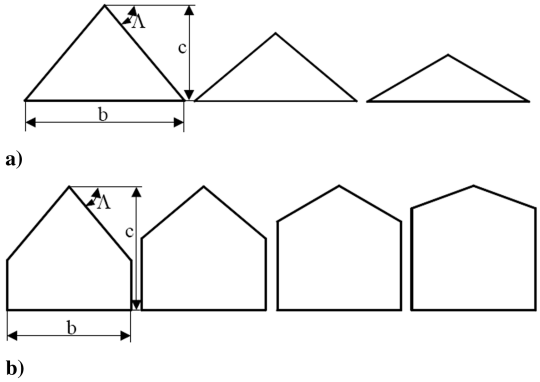

Fig. 2 Low-sweep wings tested: a) simple delta wings, and b) cropped delta wings.

wing. The rolling mechanism was composed of an electric motor (see Fig. 1) and a drive mechanism, which was used to transmit the motion smoothly. The mechanism was controlled using a desktop computer. Data acquisition software HP VEE was used to control the amplitude and frequency of the periodic sinusoidal rolling motion. The amplitude and dimensionless frequency of the rolling motion was varied in the range of $\Delta\phi = 1$–5 deg, and $fc/U_\infty = 0$–10. Experiments were carried out at a freestream velocity of $U_\infty = 0.3$ m/s, giving a Reynolds number range of $Re = 13,000$–$30,000$.

B. Techniques

Visualization of the vortical flow was performed using food coloring dye, diluted 1:4 with water. A digital video camera, with a capture rate of 25 frames per second and a resolution of 570,000 pixels, was used to capture images from the dye flow visualization, and was interfaced to a desktop computer via the commercial software package Pinnacle Studio DV, enabling real-time viewing of the wing and the capture of camera images and video recordings. The measurement uncertainty in locating the vortex breakdown position was approximately 2% of the chord length.

In addition, for the $\Lambda = 50$ deg simple delta wing, flow visualization in crossflow planes (normal to the freestream direction) above the wing model was performed using fluorescent dye, which was released from slots (of 0.5 mm thickness) near the leading edges. Different colors of fluorescent dye were used to visualize the leading-edge vortex pair, although the pictures presented in this paper are in gray levels. A 4 W Argon-Ion laser was used in these experiments. Light is transmitted via a fiber-optic cable to the optical head, and a lens is used to generate a light sheet.

Quantitative flow measurements were undertaken using digital particle image velocimetry (DPIV). Two different PIV systems were used. Most of the measurements were taken using a high-frame-rate DPIV system. Illumination of the desired plane was achieved using a New Wave Pegasus Nd:YLF double-pulse high-speed laser with a maximum energy of 10 mJ per pulse. The laser light sheet was placed parallel to the freestream velocity for the measurements in streamwise planes, and perpendicular to the freestream for the crossflow measurements. The images were captured using a TSI PowerView HS-3000 high-speed complementary metal-oxide-semiconductor (CMOS) camera. A TSI LaserPulse synchronizer unit was used to link the camera and the laser to enable the accurate capture for two frame cross-correlation analysis. For these measurements, the system was operated at 0.5 kHz, giving an area of resolution of 1024×1024 pixels. This allowed the capture of the velocity field at 0.25 kHz and 1250 instantaneous images were captured for each of the measurement planes for both the dynamic and static wing. The flow was seeded with commercially available hollow glass particles of a mean diameter of 8–12 μm. The commercial software TSI Insight3G and a fast Fourier transform (FFT) cross-correlation algorithm were used for the analysis of the results obtained. The size of the interrogation window was 32×32 pixels for the measurements in streamwise planes and 24×24 pixels for the crossflow measurements. The grid spacing varied in the range of 1–3% of the chord length in the streamwise planes, and was around 3% of the local semispan for the crossflow planes.

The second system, with which the phase-averaged measurements were taken, was a TSI Solo DPIV system. The system incorporates a pair of pulsed mini-Nd:YAG lasers with a maximum energy of 120 mJ per pulse, which was used to illuminate the plane of interest. Images were captured using an 8-bit TSI PowerView 4 M charge-coupled device digital camera with a resolution of 2048×2048 pixels and a maximum capture rate of 7.5 frames per second, producing 3.75 frames in cross correlation. A combination of cylindrical and spherical lenses was used to generate the required light sheet. For crossflow measurements, the laser light sheet was placed normal to the freestream. In addition, the light sheet was placed parallel and close to the wing surface (approximately 1 mm) to reveal the near-surface flow pattern. The commercial software package TSI Insight v6.0 and an FFT cross-correlation algorithm were used to analyze the images, with an interrogation window size of 32×32 pixels, and to produce velocity vectors for further processing. The effective grid size was 2% of the local semispan s in crossflow measurements, and around 2% of the chord length in measurements in a plane near the wing surface. The PIV system was triggered to capture the flowfield at zero roll angle and then perform phase averaging. Sequences of 30 instantaneous measurements were taken for each case and the phase-averaged velocity and vorticity fields were calculated. The measurement uncertainty for the velocity is estimated as 2% of the freestream velocity.

LDV measurements were undertaken using a 300 mW air-cooled Argon-Ion laser and TSI burst correlator unit. The same seeding particles used for the PIV measurements were also used for the LDV measurements. The data rate was on the order of 1 kHz, and a total of 6000 data points were recorded for each test. The LDV fiber-optic probe was attached to a three-axis computer controlled traverse for automated measurements. The chordwise velocity was measured in the crossflow plane at $x/c = 0.7$ as a function of vertical distance from the wing surface.

III. Results

A. Reattachment

As mentioned previously, the majority of the experiments were performed on the rigid simple delta wing with sweep angle of $\Lambda = 50$ deg and by using small-amplitude rolling motion. In these experiments, fluorescent dye was released from a slot near the leading edge, which "marked" the vorticity shed with separation. The objective was to visualize the shear layer structures. Figure 3 shows

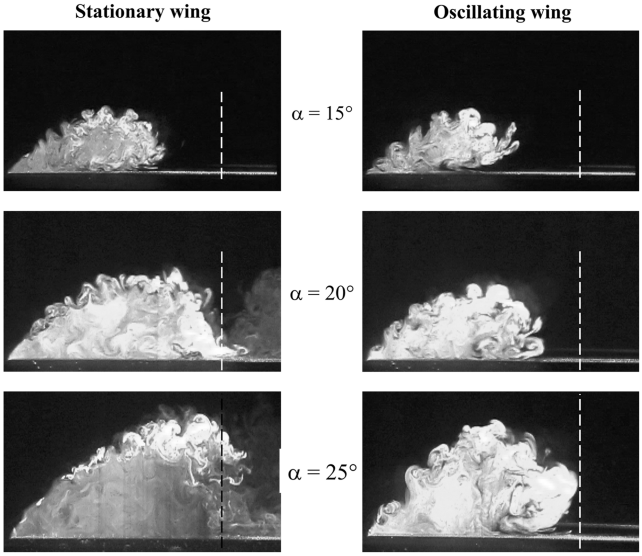

Fig. 3 Laser fluorescence flow visualization for stationary ($Sr = 0$) and oscillating wings ($Sr = 1.0$, $\Delta\phi = 1$ deg), $\Lambda = 50$ deg. Exposure time was 1/750 s.

flow visualization for the stationary and rolling delta wing (with an amplitude of $\Delta\phi = 1$ deg and Strouhal number $Sr = 1.0$) for angles of attack of $\alpha = 15$ deg (prestall), $\alpha = 20$ deg (stall), and $\alpha = 25$ deg (poststall) at $x/c = 0.8$. Dye is released from only one side of the wing in this case and the dashed vertical line indicates the wing centerline in these pictures. Although the difference between the cases of stationary and oscillating wings is small for $\alpha = 15$ deg, there is still evidence of earlier reattachment. At higher incidences of $\alpha = 20$ and $\alpha = 25$ deg, the change in the size of the vortical region is considerable for the oscillating wing due to earlier reattachment. The Strouhal number of these perturbations ($Sr = 1.0$) is close to the natural frequency of the shear layer instability (based on the previous measurements [15] of the center peak frequency from hot-wire measurements). The wavelength of the vortical structures on stationary and oscillating wings confirms that the natural frequency of the shear layer instability is indeed close to $Sr = 1$.

Figure 4 shows the time-averaged flow visualization for the three incidences under the same conditions as those in Fig. 3. In this case, the dye was released from both leading edges and at least 10 images were averaged. As seen in Figs. 3 and 4, the most dramatic results are observed for the poststall conditions at $\alpha = 25$ deg. Totally separated flow for the stationary wing at this incidence becomes reattached to the wing surface for the oscillating wing. The wing oscillations also delay the stall of the stationary wing at $\alpha = 20$ deg for which the separated shear layers just reattach at the wing centerline. The flow pattern for $\alpha = 20$ deg becomes similar to what is expected at a lower incidence for the stationary wing.

Figure 5 shows the time-averaged velocity field in a crossflow plane at $x/c = 0.5$ for the stationary and oscillating wing ($Sr = 1.5$, $\Delta\phi = 1$ deg) at $\alpha = 25$ deg. It is clear from the crossflow measurements that both shear layers meet at the wing centerline for the stationary wing and there is no reattachment to the wing surface. However, for the oscillating wing, the shear layer reattaches to the wing surface and the vortical flow appears to be more organized. The stalled flow on the stationary wing is replaced by the coherent vortical structures on the oscillating wing. The number and nature of the critical points and separation/reattachment lines are the same for the stationary and oscillating wings, but the flow becomes more organized with excitation.

For the same angle of attack and the same parameters for the oscillating wing, detailed velocity measurements were also taken in streamwise planes parallel to the freestream, as shown in the inset of Fig. 6. To understand the features of the reattachment process, flow in several planes, including ones very close to the apex of the wing were studied. As an example, Fig. 6 shows the time-averaged velocity field at $x/c = 0.15$ and 0.5 for the stationary and oscillating wing. Comparison of flowfields at $x/c = 0.15$ for the stationary and oscillating wings reveals the distinct difference. Near the wing centerline, there is a clear reattachment region for the oscillating wing. The reattachment already takes place near the apex. For the stalled flow over the stationary wing, there is no reattachment and this is easily seen in the PIV measurements in the streamwise planes. For the oscillating wing, the closed recirculation regions correspond to the leading-edge vortices in these planes which cut through the vortices a small angle. Of course, the flow pattern in this streamwise plane is different from that in a crossflow plane. Near the centerline, the flow moves away from the wing, which is a result of the attached flow near the wing surface. Note that there is no trace of a saddle point that would correspond to attachment in this plane. This is due to the fact that only the velocity component in the measurement plane is visible. Comparison of flowfields further downstream at $x/c = 0.5$ reveals a similar effect of wing oscillations on the separated flow and reattachment process.

Complementary LDV measurements were performed to investigate the effects of frequency and amplitude parameters. Figure 7a shows the variation of the time-averaged chordwise velocity as a function of vertical distance from the wing surface at the wing centerline $y/s = 0$ and $x/c = 0.7$. The velocity profiles for different Strouhal numbers are shown and compared with that of the stationary wing. The large velocity defect at the wing symmetry plane for the stationary wing diminishes with increasing Strouhal number and the velocity profile becomes almost uniform (with the exception of a thin boundary layer near the surface) at high frequencies. Figure 7b shows the chordwise velocity profiles at $y/s = 0.5$ for the same streamwise station. The velocity profiles for different amplitudes (and $Sr = 1.0$) show the nature of the axial flow in the vortical flow regions. The velocity profile is wakelike for all cases. Although the minimum velocity increases with increasing amplitude, there is no evidence of axial flow developing in the cores of the vortices, at least at this streamwise station ($x/c = 0.7$).

B. Vortex Re-formation

Figure 8 shows flow visualization for the stationary and rolling delta wing (with an amplitude of 5 deg) for an incidence of $\alpha = 25$ deg. It is seen that the totally separated flow for the stationary wing becomes very organized for the rolling wing with increasing frequency. The most interesting observations are the re-formation of the leading-edge vortices at high frequencies, and their subsequent breakdown. At relatively low Strouhal numbers, such as $Sr = 0.3$, there is only reattachment of the separated shear layers, but there is no (jetlike) axial flow in the cores of the vortices. With increasing Strouhal number, axial flow in the cores of vortices develops very close to the apex, and then breaks down. The location of vortex breakdown first increases with increasing Strouhal number, but then decreases at the highest Strouhal number ($Sr = 10$). Hence, there is evidence of an optimum Strouhal number. Flow control produces two separate effects: first is the reattachment when the frequency is small. The second stage is the vortex re-formation (with intense axial flow along the axis) at higher frequencies. Flow visualization

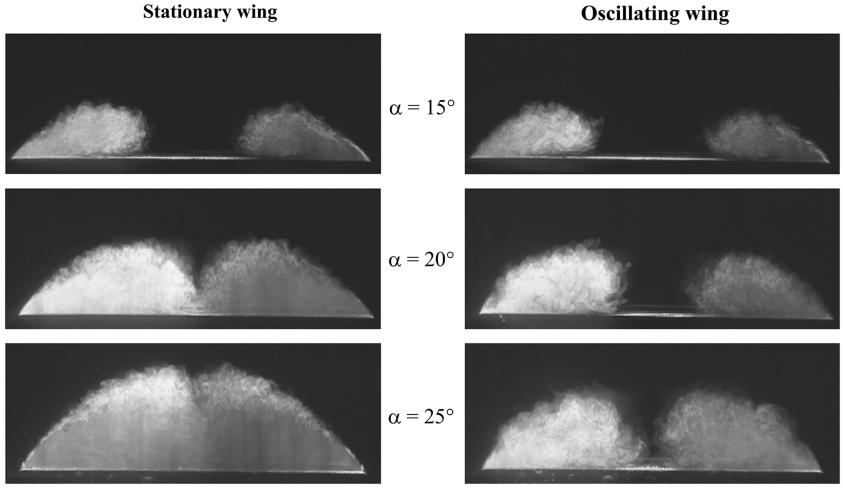

Fig. 4 Time-averaged laser fluorescence flow visualization for stationary ($Sr = 0$) and oscillating wings ($Sr = 1.0$, $\Delta\phi = 1$ deg), $\Lambda = 50$ deg.

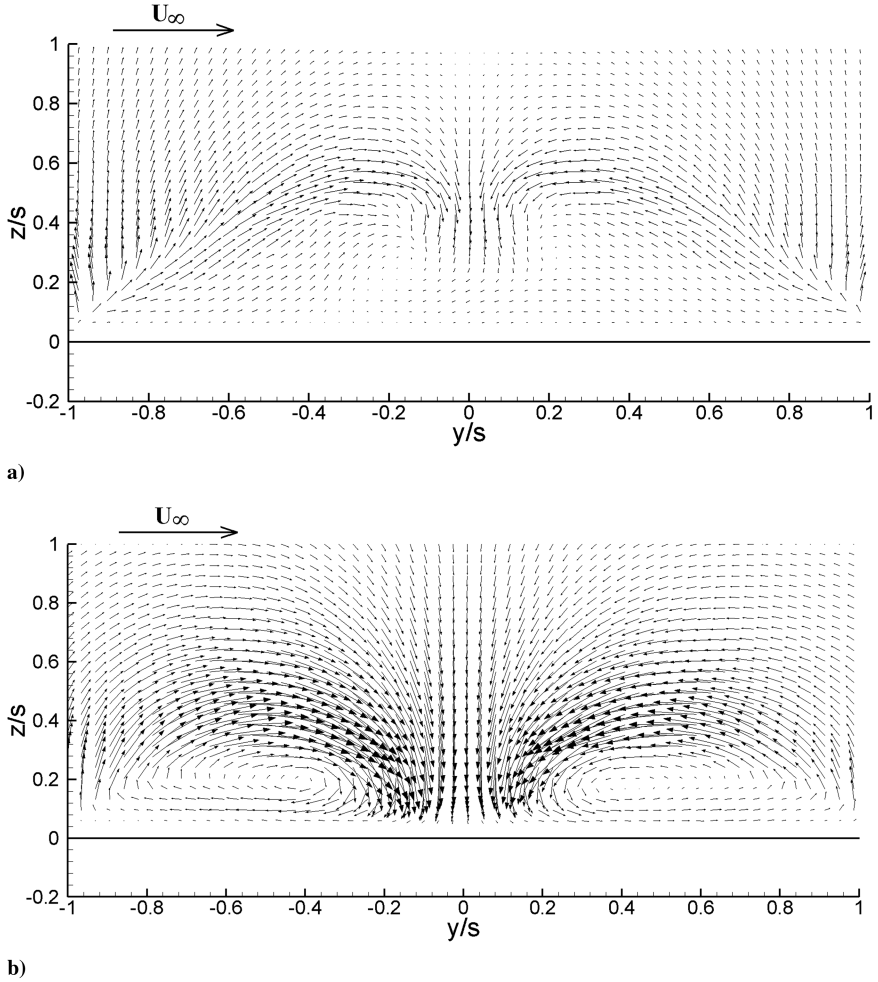

Fig. 5 Time-averaged velocity field in a crossflow plane at $x/c = 0.5$ for a) stationary ($Sr = 0$) and b) oscillating wing ($Sr = 1.5$, $\Delta\phi = 1$ deg). $\Lambda = 50$ deg, $\alpha = 25$ deg.

pictures in Fig. 8 show that vortex re-formation is not observed at low frequencies, whereas the reattachment is obvious. Only for frequencies larger than a threshold value, vortex re-formation is observed.

Figure 9 shows the variation of time-averaged breakdown location as a function of dimensionless frequency for different angles of attack in the range $\alpha = 20$–30 deg in the poststall region. It is seen that, for each incidence in the poststall region, the breakdown location is zero for the stationary wing ($fc/U_\infty = 0$) and the maximum delay of the vortex breakdown location is achieved in the range of $fc/U_\infty = 1$–2. This range of Strouhal numbers compares well with the dominant frequencies of the shear layer instabilities [7,16] for a nonslender wing of $\Lambda = 50$ deg. Figure 10 compares the variation of mean breakdown location as a function of dimensionless frequency for two amplitudes of rolling motion for $\alpha = 25$ deg. Even for the small amplitude of $\Delta\phi = 1$ deg, it is possible to have reestablished leading-edge vortices. The optimum dimensionless frequency is also in the same range.

In the case of the rigid wing undergoing small-amplitude rolling motion, the dimensionless frequency fc/U_∞ is not only a ratio of time scales of convective time and perturbations (rolling motion), but also the ratio of the leading-edge velocity and freestream velocity for a given wing. Figures 9 and 10 suggest that increasing velocity of the leading edge (with increasing frequency parameter) does not necessarily delay breakdown location any further. However, it is expected that the time-averaged vorticity flux will increase with increasing velocity of the leading edge. (The time-averaged vorticity flux is proportional to $\bar{U}_s^2$, where U_s denotes the velocity outside the boundary layer at the separation point. It is expected that this term will increase with increasing frequency as a first approximation). This is confirmed by the vorticity distributions [14] in a crossflow plane (not shown here) for $\alpha = 25$ deg. It was observed that larger values of vorticity exist for the oscillating wing. Another expected reason for the increase in the magnitude of the vorticity is the re-formation of the leading-edge vortices. The variation of circulation with the dimensionless frequency is shown in Fig. 11. The circulation was calculated as the line integral of velocity around a rectangle that encloses the vortex. It is seen that the circulation of the vortical flow in a crossflow plane increases with frequency in comparison to the stationary wing. Although the leading-edge vortices become stronger due to the leading-edge motion, vortex breakdown is delayed for the rolling wing compared with the stationary wing for which breakdown is at the apex. This appears to be in contrast to the well-known studies of vortex breakdown, which indicate that increased strength of vortices should cause premature, rather than delayed, breakdown. This result suggests that the streamwise pressure gradient might be modified favorably due to the wing motion.

A final remark will be made on the nature of the phase-averaged flow near the wing surface. Figure 12 shows the phase-averaged streamline pattern near the wing surface for different dimensionless frequencies at $\alpha = 25$ deg. The phase-averaged measurements were taken when the roll angle is zero and the right-hand side tip moves up. For the stationary wing, the flow is completely stalled, as also evidenced by the near-surface streamline pattern. For $Sr = 0.15$, there is already significant change in the flow pattern. With a further increase to $Sr = 0.3$, there is a first indication of reattached flow. With further increases in the Strouhal number, the near-surface streamline pattern changes very little and two reattachment lines are always identified. The effect of frequency was presented in more

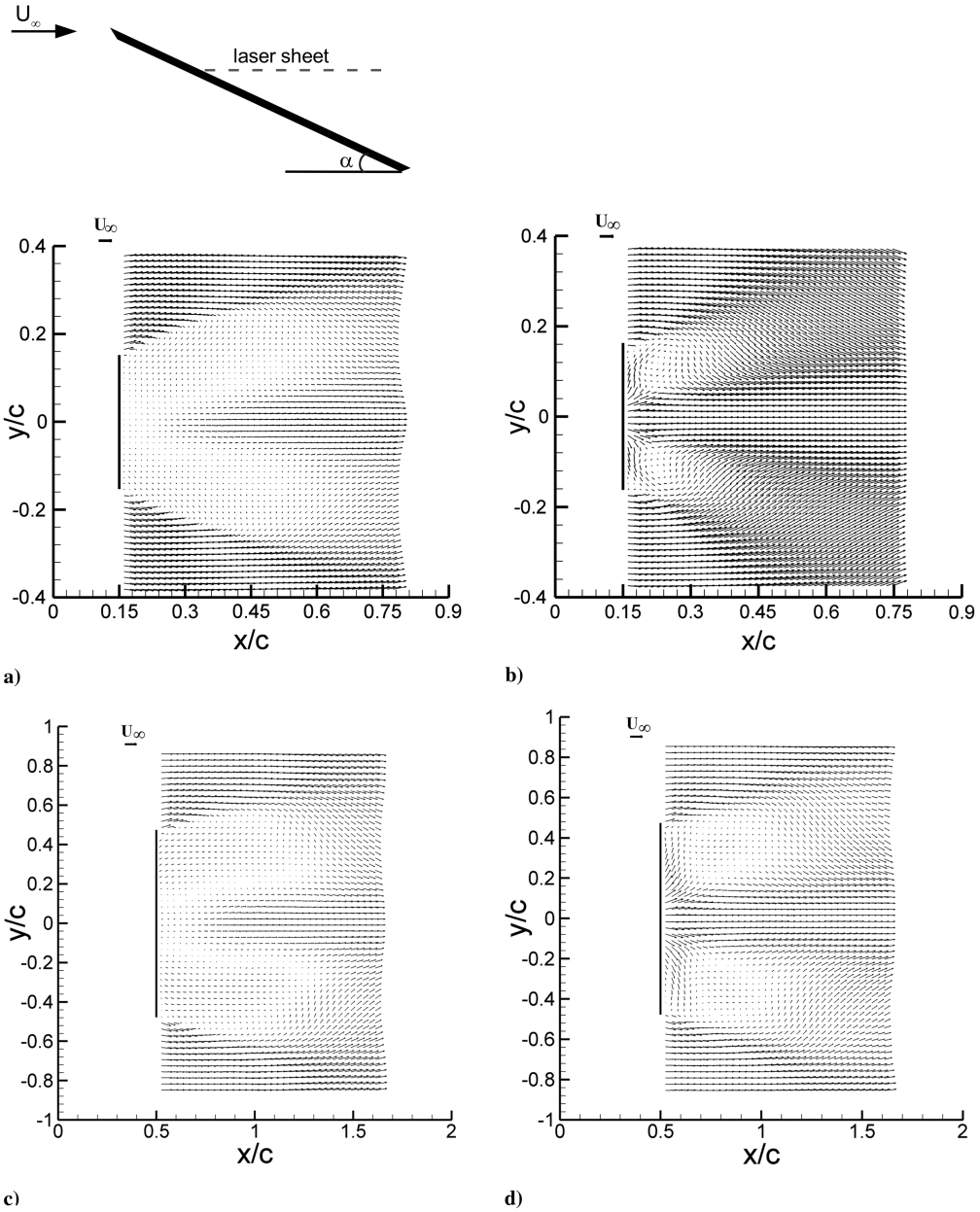

Fig. 6 Time-averaged velocity field in a streamwise plane at $x/c = 0.15$ for a) $Sr = 0$, b) $Sr = 1.5$, and at $x/c = 0.5$ for c) $Sr = 0$, d) $Sr = 1.5$. $\Lambda = 50$ deg, $\alpha = 25$ deg, $\Delta\phi = 1$ deg.

detail in the Ph.D. thesis of the first author [17]. The spanwise distance between the reattachment lines appear to increase with frequency, although there is evidence of a slight decrease at the highest frequencies. The reattachment appears to start from the apex of the wing, which is different than the case of a flexible wing [12] (where there is a node of attachment at around $x/c = 0.2$ on the centerline).

C. Effect of Wing Sweep Angle

Wing sweep angle is believed to be an important parameter. The effect of excitation on a swept wing is similar to the response of the flow over a backward-facing step [18] to the periodic excitation. However, for zero sweep angle, formation of a stable separation bubble at high angles of attack in the poststall region is not possible. It seems that a moderate sweep angle (such as 50 deg) helps the formation of semiclosed separation bubbles, hence the wing sweep is beneficial in flow reattachment. However, there must be a lower limit of sweep angle below which the beneficial effect of wing sweep will diminish. This has been investigated in systematic experiments as explained next.

Extensive flow visualization for the oscillating delta wings with $\Lambda = 40$ deg and $\alpha = 30$ deg has been conducted [17]. Examples of flow visualization pictures for $Sr = 0$ and $Sr = 1.2$ are shown in Fig. 13 at different incidences for small-amplitude rolling motion ($\Delta\phi = 5$ deg). For $\Lambda = 40$ deg and $\alpha = 15$ deg, there is reattachment, although breakdown is at the apex for the stationary wing. Reformation of the leading-edge vortices and vortex breakdown are visible for the oscillating wing. It was shown in [17] that, for the largest incidence $\alpha = 25$ deg, completely stalled flow for the stationary wing becomes reattached with wing oscillations for this sweep angle.

For the oscillating wing, it is seen that, at higher incidences, vortex breakdown is at the apex but flow reattachment is still possible. To quantify the effect of excitation on the stalled flow, the quantity Δy_w was defined as the distance between the breakdown wakes at midchord, as shown in Fig. 14a. As the reattachment location is slightly inboard of the leading-edge vortex, the breakdown wake gives an indication of the reattachment line. Although this is not exactly related to the reattachment line, it gives a measure of the effect of excitation on flow. For example, when the distance between the breakdown wakes is zero, the flow is stalled. The variation of this

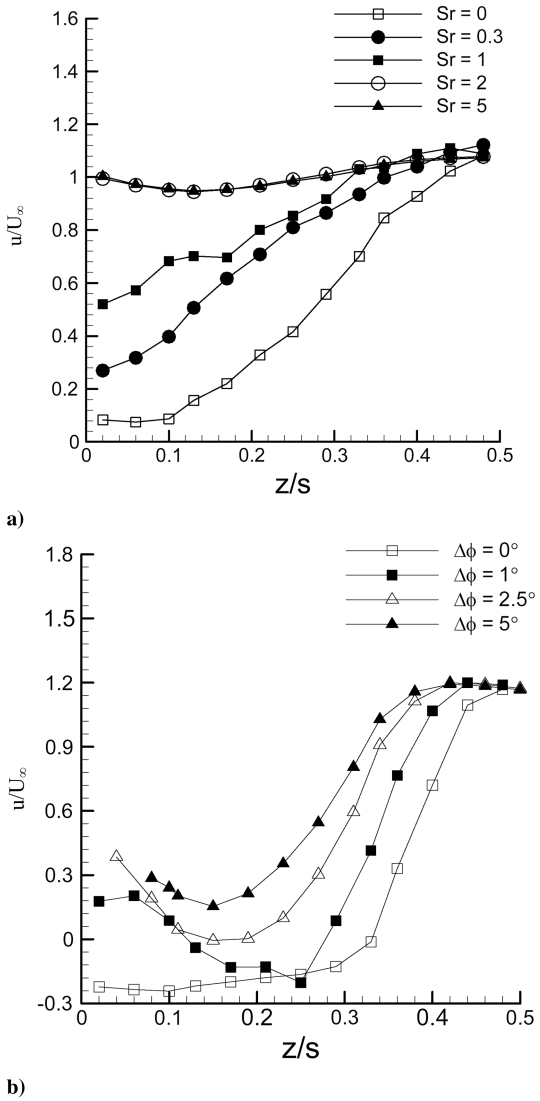

Fig. 7 Time-averaged chordwise velocity profiles as a function of vertical distance from the wing surface at $x/c = 0.7$ and a) $y/s = 0$ for different dimensionless frequencies, $\Delta\phi = 1$ deg, and b) $y/s = 0.5$ for different amplitudes, $Sr = 1.0$. $\Lambda = 50$ deg, $\alpha = 25$ deg.

quantity is related to the movement of the reattachment line. This quantity is useful for the cases when the flow is close to the stall (when the breakdown location is close to the apex and difficult to measure). Figure 14b shows the variation of this parameter as well as breakdown location as a function of dimensionless frequency at $\alpha = 15$ deg. It is seen that the variation of this parameter is very similar to that of the breakdown location, and both curves show a peak around the same optimum frequency. Figure 14b shows the variation of the parameter Δy_w as a function of dimensionless frequency at three different incidences. It is seen that optimum frequencies for all three cases are around $Sr = 1$.

Results for $\Lambda = 30$ deg are generally similar. An example is shown in Fig. 13. In [17], detailed results are presented. It was found that, in all cases, except for the largest angle of attack $\alpha = 25$ deg, flow reattachment occurs over the wing for the roll oscillations at $Sr = 1.2$. Figure 15 shows the variation of the parameter Δy_w as a function of dimensionless frequency for $\alpha = 10$, 15, and 20 deg. Again, the "optimum frequency" is around $Sr = 1$, which is similar to the results for $\Lambda = 50$ deg and $\Lambda = 40$ deg delta wings. A distinct feature for the largest incidence $\alpha = 20$ deg is observed in Fig. 15; for frequencies much higher than the optimum frequency, the flow reattachment becomes impossible.

These experiments for $\Lambda = 30$, 40, and 50 deg indicated that the reattachment process is generic for all nonslender wings and there is an optimum frequency range of $fc/U_\infty = 1$–2. As discussed earlier,

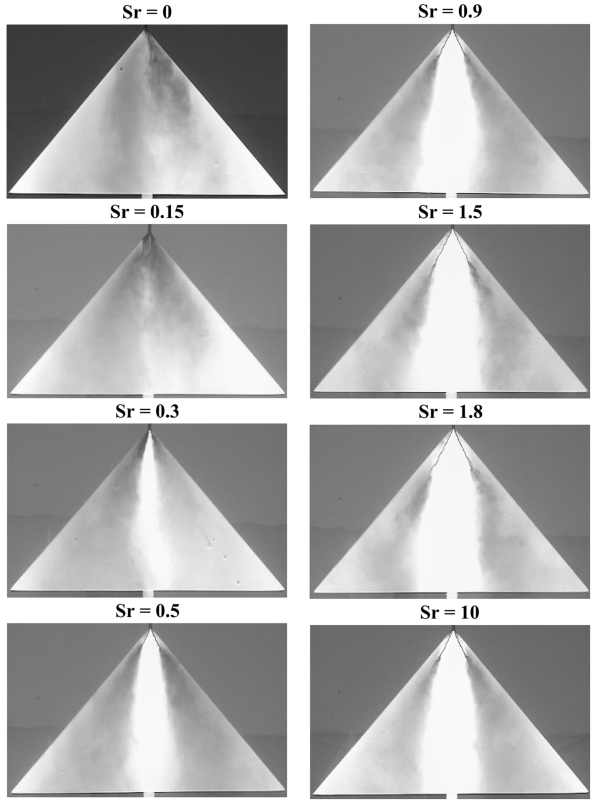

Fig. 8 Flow visualization for a stationary and small-amplitude ($\Delta\phi = 5$ deg) rolling wing. $\Lambda = 50$ deg, $\alpha = 25$ deg.

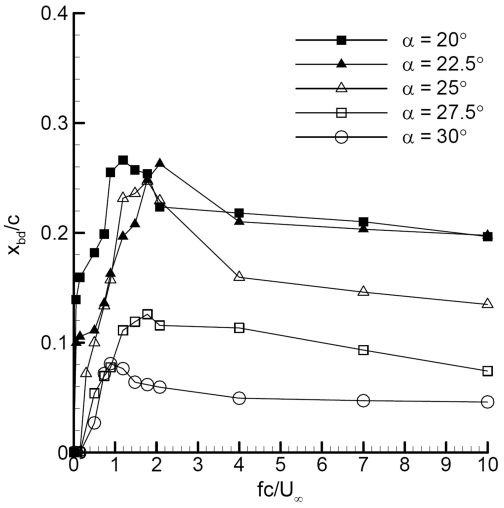

Fig. 9 Variation of the mean breakdown location as a function of dimensionless frequency Sr for different incidences. $\Lambda = 50$ deg, $\Delta\phi = 5$ deg.

this is believed to be a feature of nonslender wings ($\Lambda \leq 55$ deg). For slender wings ($\Lambda \leq 65$ deg), reattachment is not likely to be on the wing surface. For sweep angles in between 55 and 65 deg, the unsteady excitation might still be useful. For $\Lambda = 60$ deg, which is a transitional case between the slender and nonslender wings, there is evidence [9,19] that a similar range of forcing frequencies promote reattachment.

D. Effect of Wing Planform Shape

Cropped delta wings were studied to investigate the effect of planform shape on the results, in particular, on the optimum frequency. Figure 13 shows some examples of flow visualization

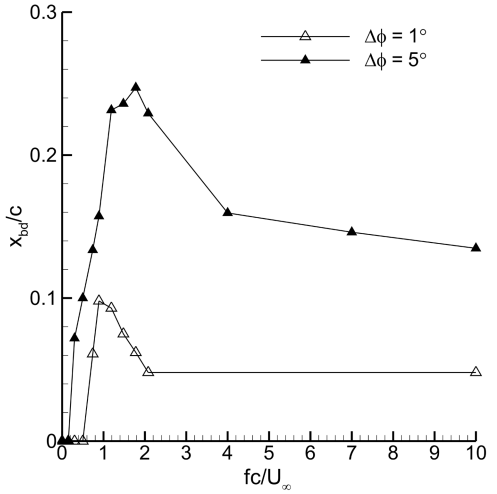

Fig. 10 Variation of time-averaged breakdown location as a function of dimensionless frequency for two values of oscillation amplitude, $\Lambda = 50$ deg, $\alpha = 25$ deg.

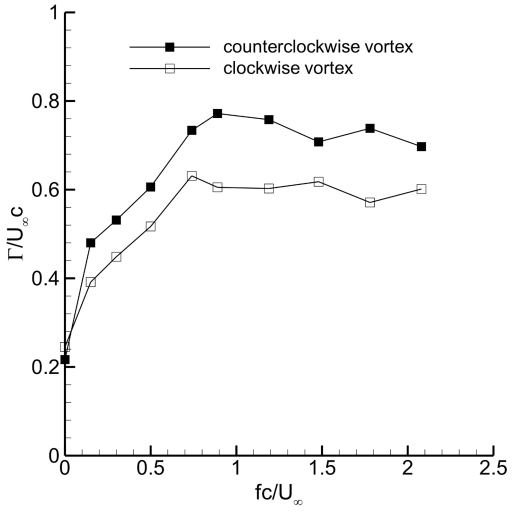

Fig. 11 Variation of normalized circulation of vortical flow in a crossflow plane at $x/c = 0.8$ as a function of dimensionless frequency, $\Lambda = 50$ deg, $\alpha = 25$ deg, $\Delta\phi = 5$ deg.

pictures for cropped delta wings with $\Lambda = 50$, 40, and 30 deg at various incidences. Qualitatively, the results appear very similar to those of simple delta wings with the same sweep angle. Figure 16 shows the variation of the parameter Δy_w as a function of the dimensionless frequency parameter for $\alpha = 25$ deg. For comparison, the variation of breakdown location for the simple delta wing at the same angle of attack is added into Fig. 16. It is seen that the results are very similar, and indicate optimum frequencies in the range of $Sr = 1$–2.

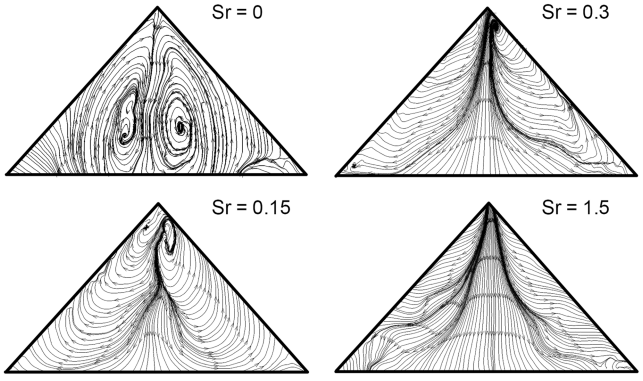

Fig. 12 Near-surface streamline patterns for different dimensionless frequencies, for $\Lambda = 50$ deg, $\alpha = 25$ deg, $\Delta\phi = 5$ deg.

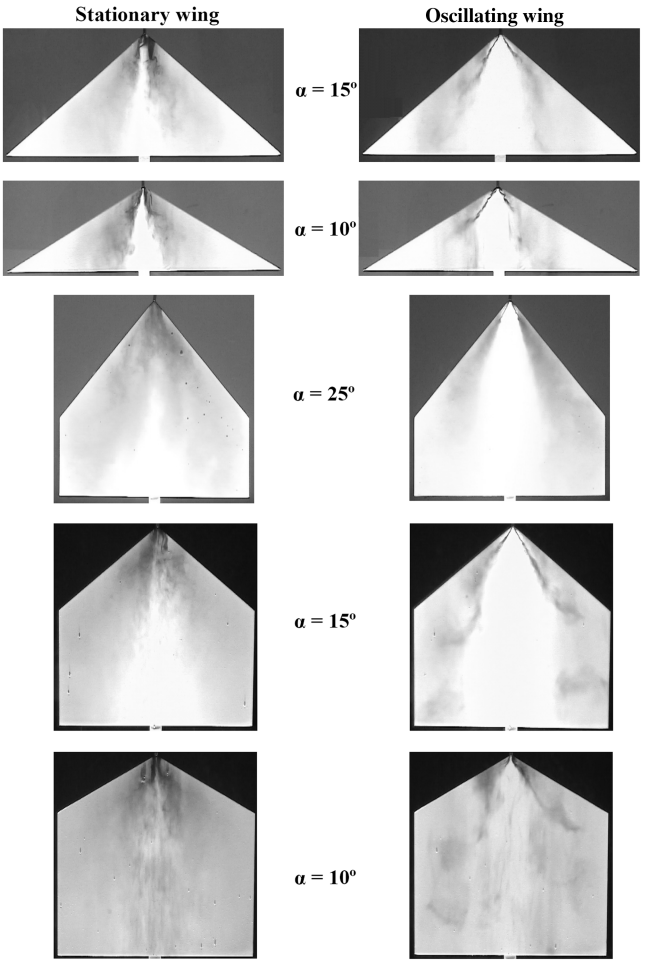

Fig. 13 Flow visualization for various wings for stationary and oscillating motion. Strouhal numbers are $Sr = 1.2$ for 40 and 30 deg delta, 50 deg cropped delta, and $Sr = 2.0$ for 40 and 30 deg cropped delta. $\Delta\phi = 5$ deg.

The effect of wing oscillations for cropped delta wings with $\Lambda = 40$, 30, and 20 deg is reported in detail in the thesis [17] of the first author. For $\Lambda = 40$ and 30 deg, earlier reattachment at low incidences and reattachment of completely stalled flow at higher incidences are very similar to previous observations for other wings. Again, excitation at $Sr = 1$–2 appears to be effective. Here, we show an example for each wing in the poststall region in Fig. 13. However, for $\Lambda = 20$ deg, it has been found [17] that wing oscillations do not cause reattachment. Hence, it appears that the lower limit of sweep angle below which the beneficial effect of wing sweep diminishes is around $\Lambda = 20$ deg.

E. Symmetric vs Antisymmetric Wing Oscillations

Finally, previous work [10–12] has suggested the importance of antisymmetric perturbations as the wing vibrations occurred at an antisymmetric mode. It was shown that a half-model delta wing did not exhibit self-excited vibrations. Hence, one of the remaining unresolved issues is the role of the antisymmetric perturbations and whether they are essential for reattachment, vortex re-formation, and lift enhancement.

To investigate the effect of symmetric perturbations vs antisymmetric perturbations, it is necessary to employ symmetric wing oscillations. Symmetric perturbations in the form of small-amplitude pitching oscillations (amplitude $\Delta\alpha = 1$ deg) were studied for $\Lambda = 50$ deg simple delta wing. Here, the pitching axis was located at

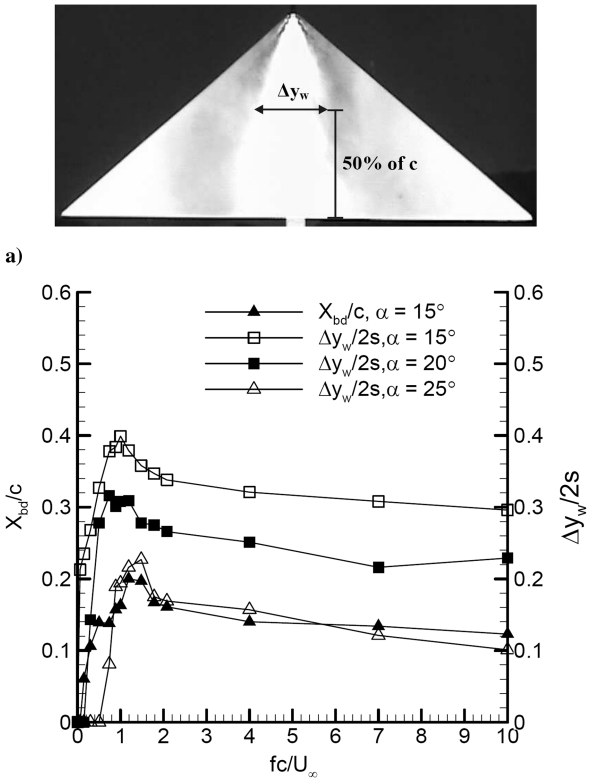

Fig. 14 Distance between the breakdown wakes Δy_w at midchord: a) definition of flow visualization picture, b) its variation as a function of dimensionless frequency for $\Lambda = 40$ deg delta wing. $\Delta\phi = 5$ deg.

1.12c downstream of the wing. The results of flow visualization are shown in Fig. 17 for $\alpha = 25$ deg. Again, earlier reattachment and even the re-formation of the leading-edge vortex are observed for increasing dimensionless frequency for the oscillating wing. Hence, for active control purposes, both symmetric and antisymmetric forcing would work. However, passive control for a flexible wing occurs only in the antisymmetric mode. Figure 18 shows a comparison of the variations of breakdown location as a function of dimensionless frequency for the pitch and roll oscillations with the same amplitude of 1 deg. Small-amplitude symmetric oscillations appear to be more effective, however, it is not possible to make a direct comparison of which forcing mechanism (symmetric vs

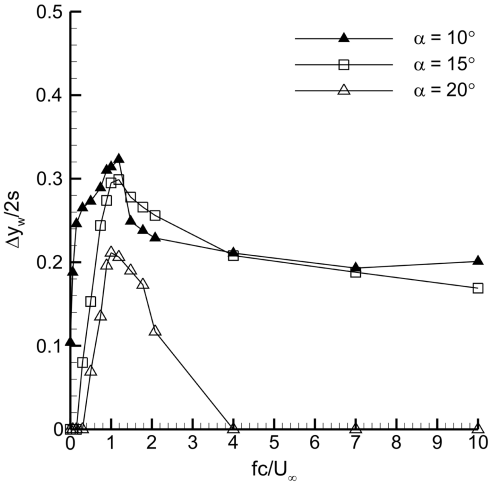

Fig. 15 Variation of mean distance between the breakdown wakes Δy_w as a function of the dimensionless frequency at different incidences for $\Lambda = 30$ deg delta wing. $\Delta\phi = 5$ deg.

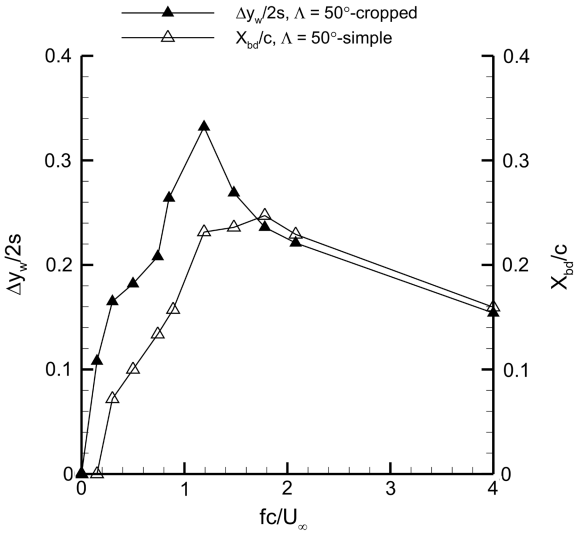

Fig. 16 Variation of breakdown location and distance between the breakdown wakes Δy_w as a function of the dimensionless frequency at $\alpha = 25$ deg for $\Lambda = 50$ deg cropped and simple delta wings. $\Delta\phi = 5$ deg.

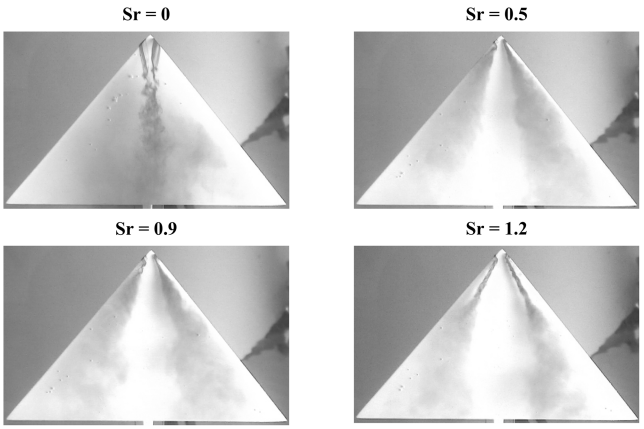

Fig. 17 Effect of dimensionless frequency Sr on $\Lambda = 50$ deg delta wing at $\alpha = 25$ deg for small-amplitude ($\Delta\alpha = 1$ deg) pitching motion.

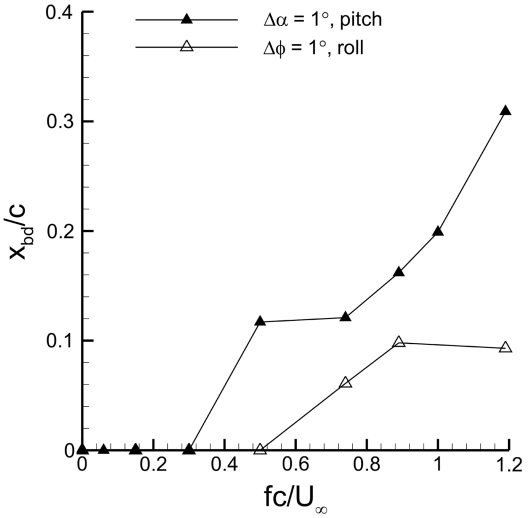

Fig. 18 Variation of the mean breakdown location as a function of the dimensionless frequency at $\alpha = 25$ deg for $\Lambda = 50$ deg for small-amplitude pitching and rolling motions.

antisymmetric) is more efficient, as the leading-edge velocity perturbations are vastly different in their geometric form. Nevertheless, the results show that symmetric perturbations also promote reattachment and vortex re-formation. Yaniktepe and Rockwell [5] showed that, for an even lower sweep angle of $\Lambda = 38.7$ deg, the effect of small perturbations (1 deg pitching oscillations) is substantial for $\alpha = 17$ deg, which is in the poststall region for the stationary wing.

IV. Conclusions

Effects of small-amplitude wing oscillations on flow reattachment and vortex re-formation in the poststall region were investigated experimentally in a water-tunnel study. Low-aspect-ratio delta and cropped delta wings with sweep angles in the range of $\Lambda =$ 20–50 deg were tested. Flow visualization, particle image velocimetry and laser Doppler velocimetry measurements were used to study the unsteady aerodynamics of oscillating wings. Effects of forcing frequency, amplitude, wing sweep angle, and mode of the wing oscillations were investigated.

Although wing oscillations promote the earlier attachment of the separated shear layer at prestall incidences, reattachment of the otherwise separated flow at poststall incidences is more remarkable. Totally separated flow for the stationary wing at poststall incidences becomes reattached to the wing surface for the oscillating wing. Flow visualization and PIV measurements indicate that reattachment starts very close to the apex when the frequency of the perturbations is close to the natural frequency of the shear layer instability.

A more interesting observation was the re-formation of the leading-edge vortices with increasing frequency. Axial flow develops in the cores of the vortices close to the apex, followed by their breakdown. For an optimum range of Strouhal numbers, $Sr = 1$–2, vortex breakdown is delayed to a maximum distance from the apex. This range of Strouhal numbers compares well with the dominant frequencies of the shear layer instabilities. The time-averaged vorticity flux and the circulation of the vortices increase with increasing velocity (or frequency) of the leading-edge oscillations.

The experiments for $\Lambda = 30$, 40, and 50 deg indicated that the reattachment process is generic for all nonslender wings and there is an optimum frequency range of $fc/U_\infty = 1$–2. However, there is a lower limit of sweep angle below which reattachment was not observed for small-amplitude wing oscillations. This lower limit is around $\Lambda = 20$ deg. Finally, symmetric wing perturbations (pitch oscillations) are as effective as antisymmetric wing perturbations (roll oscillations) in the poststall region, and promote reattachment and re-formation of the vortices. Hence, for active control purposes, both symmetric and antisymmetric forcing would work. However, passive control for a flexible wing occurs only in the antisymmetric mode. Exploitation of these results for low-aspect-ratio wings, in the form of leading-edge vibrations, oscillatory blowing, or piezoelectric actuators, should be beneficial.

Acknowledgments

This work is supported by the European Office of Aerospace Research and Development, U.S. Air Force Office of Scientific Research, U.S. Air Force Research Laboratory, under Contract No. F61775-02-C4024. The authors would like to acknowledge additional support from the Engineering and Physical Sciences Research Council Academic Fellowship in Unmanned Air Vehicles and the Engineering and Physical Sciences Research Council grant EP/C015258/1.

References

[1] Rockwell, D., "Three-Dimensional Flow Structure on Delta Wings at High Angle-of-Attack: Experimental Concepts and Issues," *31st AIAA Aerospace Sciences Meeting & Exhibit*, AIAA Paper 93-0050, 1993.

[2] Visbal, M. R., "Computational and Physical Aspects of Vortex Breakdown on Delta Wings," *33rd AIAA Aerospace Sciences Meeting & Exhibit*, AIAA Paper 95-0585, 1995.

[3] Delery, J. M., "Aspects of Vortex Breakdown," *Progress in Aerospace Sciences*, Vol. 30, No. 1, 1994, pp. 1–59. doi:10.1016/0376-0421(94)90002-7

[4] Delery, J. M., "Physics of Vortical Flows," *Journal of Aircraft*, Vol. 29, No. 5, 1992, pp. 856–876.

[5] Yaniktepe, B., and Rockwell, D., "Flow Structure on a Delta Wing of Low Sweep Angle," *AIAA Journal*, Vol. 42, No. 3, March 2004, pp. 513–523. doi:10.2514/1.1207

[6] Taylor, G., and Gursul, I., "Buffeting Flows over a Low Sweep Delta Wing," *AIAA Journal*, Vol. 42, No. 9, Sept. 2004, pp. 1737–1745.

[7] Gursul, I., Gordnier, R., and Visbal, M., "Unsteady Aerodynamics of Nonslender Delta Wings," *Progress in Aerospace Sciences*, Vol. 41, No. 7, 2005, pp. 515–557. doi:10.1016/j.paerosci.2005.09.002

[8] Gursul, I., Wang, Z., and Vardaki, E., "Review of Flow Control Mechanisms of Leading-Edge Vortices," *Progress in Aerospace Sciences*, Vol. 43, Nos. 7–8, 2007, pp. 246–270. doi:10.1016/j.paerosci.2007.08.001

[9] Margalit, S., Greenblatt, D., Seifert, A., and Wygnanski, I., "Delta Wing Stall and Roll Control Using Segmented Piezoelectric Fluidic Actuators," *Journal of Aircraft*, Vol. 42, No. 3, 2005, pp. 698–709.

[10] Taylor, G. S., and Gursul I., "Lift Enhancement over a Flexible Low Sweep Delta Wing," *2nd AIAA Flow Control Conference*, AIAA Paper 2004-2618, 2004.

[11] Taylor, G. S., Kroker, A., and Gursul, I., "Passive Flow Control over Flexible Nonslender Delta Wings," *43rd Aerospace Sciences Meeting and Exhibit*, AIAA Paper 2005-0865, 2005.

[12] Taylor, G., Wang, Z., Vardaki, E., and Gursul, I., "Lift Enhancement over Flexible Nonslender Delta Wings," *AIAA Journal*, Vol. 45, No. 12, 2007, pp. 2979–2993. doi:10.2514/1.31308

[13] Yavuz, M. M., Elkhoury, M., and Rockwell, D., "Near-Surface Topology and Flow Structure on a Delta Wings," *AIAA Journal*, Vol. 42, No. 2, Feb. 2004, pp. 332–340.

[14] Vardaki, E., Gursul, I., and Taylor, G., "Physical Mechanisms of Lift Enhancement for Flexible Delta Wings," *43rd Aerospace Sciences Meeting and Exhibit*, AIAA Paper 2005-0867, 2005.

[15] Gursul, I., Vardaki, E., and Wang, Z., "Active and Passive Control of Reattachment on Various Low-Sweep Wings," *44th AIAA Aerospace Sciences Meeting and Exhibit*, AIAA Paper 2006-506, 2006.

[16] Gordnier, R. E., and Visbal, M. R., "Compact Differences Scheme Applied to Simulation of Low-Sweep Delta Wing Flow," *AIAA Journal*, Vol. 43, No. 8, Aug. 2005, pp. 1744–1752.

[17] Vardaki, E., "Aerodynamics of Nonslender Delta Wings," Ph.D. Thesis, Univ. of Bath, Dept. of Mechanical Engineering, Bath, England, U.K., 2006.

[18] Roos, F. W., and Kegelman, J. T., "Control of Coherent Structures in Reattaching Laminar and Turbulent Shear Layers," *AIAA Journal*, Vol. 24, No. 12, Dec. 1986, pp. 1956–1963.

[19] Gad-el-Hak, M., and Blackwelder, R. F., "Control of the Discrete Vortices from a Delta Wing," *AIAA Journal*, Vol. 25, No. 8, 1987, pp. 1042–1049.

E. Gutmark
Associate Editor